Quantum anomalous Hall effect and gate-controllable topological phase transition in layered $EuCd_2As_2$

Chengwang Niu, Ning Mao, Xiangting Hu, Baibiao Huang, and Ying Dai*
School of Physics, State Key Laboratory of Crystal Materials, Shandong University, Jinan 250100, China

(Received 21 January 2019; published 10 June 2019)

While the search for quantum anomalous Hall (QAH) insulators remains active, attention is also being paid to the controllable topological phase transitions, as they could enable the realization of both exotic quantum phenomena and novel spintronic devices. However, stable QAH insulators are innately rare to report since ferromagnetism often accompanies metallicity. Here we identify theoretically the realization of QAH effect in a stable two-dimensional ferromagnetic insulator, $EuCd_2As_2$ quintuple layers, as evidenced by the analysis of Chern number and chiral edge states. Remarkably, under electric field, a topological phase transition between QAH insulator and quantum spin Hall (QSH) insulator is revealed with the calculated nontrivial spin Chern number and Wannier charge centers for the QSH insulator. Unlike the conventional QSH insulator, here gapless edge states survive even though the time-reversal symmetry is broken by the ferromagnetic ordering. Our findings not only extend the advanced concepts but also afford exciting opportunities for experimental engineering and implementations of magnetic topological states.

DOI: 10.1103/PhysRevB.99.235119

Magnetic topological states, as fertile ground for exotic properties and for innovative design of next-generation spintronic devices, have drawn enormous interest in recent years [1,2]. The topological states are characterized by nonzero topological invariants and gapless surface/edge states [3–5]. The first experimental realization of topological states is the quantum Hall effect, which is characterized by a quantized Hall conductance $\sigma_{xy} = \mathcal{C}e^2/h$, where $\mathcal{C}$ is the Chern number, and $\mathcal{C}$ number of chiral edge states [6], in a two-dimensional (2D) electron gas under strong magnetic field. Interestingly, similar topological characters can be achieved even without external magnetic field, called quantum anomalous Hall (QAH) effect [7], which provides great potential application for dissipationless electronic and spintronic devices [8–10].

However, the progress on the QAH effect was comparatively slow until the discovery of the quantum spin Hall (QSH) effect, protected by the time-reversal symmetry ($\mathcal{T}$) and characterized by Z_2 invariant and helical gapless edge states [11,12]. In general, the QSH insulator exists in 2D materials without magnetization and its helical edge states can be viewed as two copies of the chiral edge states in the QAH insulator [13]. When $\mathcal{T}$ is broken in the QSH insulator usually by a magnetic impurity or substrate, the QSH insulator can be switched into the QAH insulator [8–10]. Nowadays, extensive investigations have been performed and numerous candidates have been theoretically predicted to host the QAH effect from the QSH insulators [14–25]. Experimentally, based on the prediction, the QAH effect is indeed confirmed in Cr-doped $(Bi, Sb)_2Te_3$ [26,27], but extreme requirements, such as the highly precise controlling of the extrinsic impurities and the ultralow temperature because of the small bulk energy gap, are required, which greatly obstructs their further device applications. To improve the feasibility of experimental realization and possible applications, 2D layered ferromagnetic insulators are good candidates and deserve to be investigated in experiment and theory.

On the other hand, topological phase transition has attracted enormous interest as it provides great insight into both the fundamental understanding and the future use of topological states [28–37]. However, the topological phase transition between QSH and QAH states is investigated only in toy models by mimicking an exchange field, and efficient methods of fast on/off switching of the QSH and QAH states are still lacking [38]. In particular, a gap opens up at the edge states of the QSH insulator when $\mathcal{T}$ is broken before the QAH effect is obtained [39]. Therefore, a natural question arises as to whether the QSH effect with gapless edge states is possible in the $\mathcal{T}$-broken QSH insulator? It gives rise to a topological phase that is different from the conventional QSH insulator.

In the present work, we report the identification of a topological phase transition between QAH and $\mathcal{T}$-broken QSH effects, and interestingly, the gapless edge states are indeed obtained in the resulted $\mathcal{T}$-broken QSH insulator, by means of the first-principles calculations taking $EuCd_2As_2$ QLs as an example. $EuCd_2As_2$ QLs is a stable 2D ferromagnets with a band gap of 72 meV. The calculated Chern number $\mathcal{C} = 1$ and chiral edge states confirm the QAH effect clearly. While this finding is interesting by itself, under electric field, we further demonstrate the possibility of the $\mathcal{T}$-broken QSH phase by a topological phase transition from the QAH effect. Topological properties of such a $\mathcal{T}$-broken QSH phase include integer spin Chern number $\mathcal{C}_S = 1$ and a pair of gapless helical edge states. These results expand the realm of topological states in 2D ferromagnetic insulators, offering a platform for exploring physics and potential applications in topological spintronics.

The density functional calculations are performed for structural relaxations and electronic structure calculations as

*daiy60@sdu.edu.cn

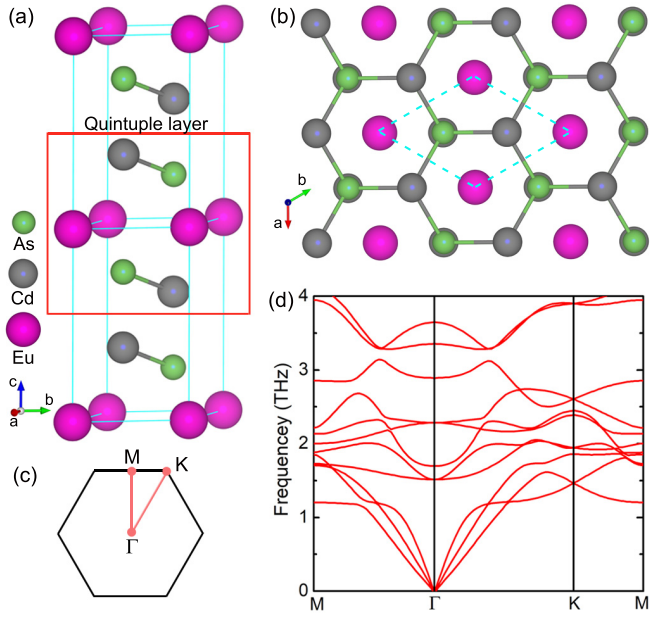

FIG. 1. (a) Crystal structure of bulk $EuCd_2As_2$ in space group $P\bar{3}m1$. Quintuple layers (QLs) constitute the simplest thin film in an ideal stoichiometry is indicated by the red square. (b) Top view of the QLs with the unit cell indicated by the dashed lines. (c) 2D Brillouin zones for the unit cell. (d) Phonon dispersion of $EuCd_2As_2$ QLs, suggesting that the QLs are dynamically stable.

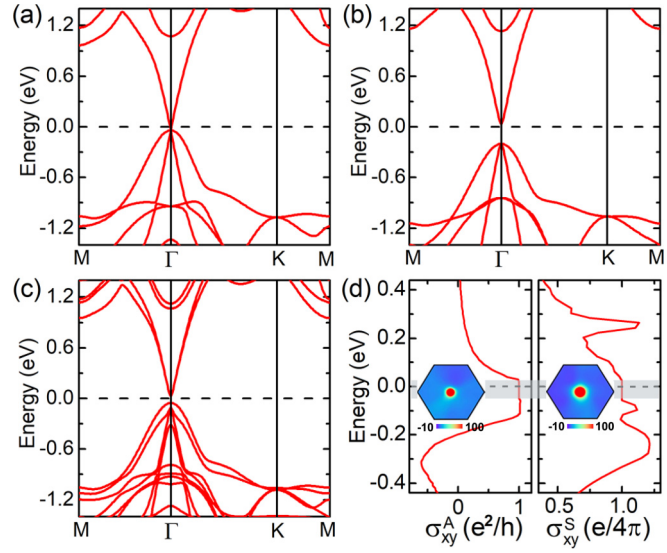

FIG. 2. Band structures of $EuCd_2As_2$ QLs (a), (b) without SOC and (c) with SOC. The (a) spin-up bands are gapless while a gap appears in the (b) spin-down bands. (d) Anomalous Hall conductivity σ^A_{xy} and spin Hall conductivity σ^S_{xy} with respect to the position of the Fermi energy E_F. Insets are Berry curvature and spin Berry curvature in the Brillouin zone. Quantized value in the SOC gap is obtained for both σ^A_{xy} and σ^S_{xy} with the main contribution around Γ.

implemented in the Vienna *ab initio* simulation package (VASP) [40,41] and the FLEUR code [42]. The generalized gradient approximation (GGA) of Perdew-Burke-Ernzerhof (PBE) is used for the exchange correlation potential [43]. Spin-orbit coupling is included in the calculations self-consistently. A vacuum layer of 20 Å is used to avoid interactions between nearest slabs for VASP while the film calculations are carried out with the film version of the FLEUR code. The phonon calculations are carried out by using the density functional perturbation theory as implemented in the PHONOPY package [44]. The maximally localized Wannier functions (MLWFs) are constructed using the wannier90 code in conjunction with the FLEUR package [45,46]. With the MLWFs, the spin Hall conductivity, anomalous Hall conductivity, Chern number, spin Chern number, Wannier charge centers, and edge states are calculated.

The layered rare-earth pnictides are of interest owing to their magnetic and thermoelectric properties [47], and recently extend to exotic topological states, such as the Dirac semimetal in magnetic $EuCd_2As_2$ [48]. Bulk $EuCd_2As_2$ has a trigonal structure with space group $P\bar{3}m1$ [49,50]. As shown in Fig. 1(a), the crystal structure can be visualized as a stacking of quintuple layers (QLs), in which CdAs layers are separated by trigonal Eu layers, along the z direction. The magnetic moments about 6.9 μ_B are localized on the Eu atom with an electronic configuration of $4f^7$, and the interlayer Eu atoms are coupled by an antiferromagnetic ordering, while a ferromagnetic (FM) ordering for the intralayer ones [48,50]. Here, we focus on the 2D $EuCd_2As_2$ QLs, shown in Fig. 1(b), which adopts the hexagonal lattice, Fig. 1(c). Its optimized lattice constant is $a = 4.48$ Å, almost the same as with experimental bulk structure [49,50]. Remarkably, the calculated cleavage energy of the QLs, ∼33 meV/Å^2, is comparable to that of MoS_2 (∼26 meV/Å^2) [51], suggesting that the $EuCd_2As_2$ QLs may be obtained in a similar way as that for MoS_2. The dynamic stability is further investigated through the phonon spectrum calculations. All phonon frequencies are positive in the entire Brillouin zone as shown in Fig. 1(d), suggesting that the $EuCd_2As_2$ QLs is dynamically stable. Then, we substantiate the thermal stability by carrying out molecular dynamics (MD) calculations [52]. There is neither bond breakage nor structure reconstruction, thus $EuCd_2As_2$ has a thermally stable structure.

Similar to the bulk form, magnetic moments of $EuCd_2As_2$ QLs at intralayer Eu sites couple ferromagnetically, which is energetically preferred by 0.6 meV, with a calculated value of 6.9 μ_B. Spin polarization occurs when the half-filled Eu-$4f$ orbitals are distributed far below (∼−1.6 eV) the Fermi energy, while the states around the Fermi energy are mainly contributed by As-s/p and Cd-s/p. The corresponding band structures are illustrated in Figs. 2(a) and 2(b); the spin-up bands are gapless while a gap appears in the spin-down bands, indicating a good half-metallic characteristic near the Fermi energy. Taking SOC into account, magnetic anisotropic energy (MAE), defined as the total-energy difference between spin orientations aligned in-plane and out-of-plane directions, is carefully checked. The results show that the out-of-plane magnetization is energetically preferred with a magnitude 3.0 meV, making the out-of-plane magnetization stable and not easy to be changed. Remarkably, the calculated band structures in Fig. 2(c) show that the SOC opens a gap of 72 meV for the spin-up bands, implying the nontrivial topology in 2D FM insulator $EuCd_2As_2$ QLs.

To show this explicitly, we calculate the anomalous Hall conductivity with $\sigma_{xy}^{A} = \mathcal{C}e^2/h$, where $\mathcal{C}$ is the Chern number given by $\mathcal{C} = \frac{1}{2\pi}\int_{\mathrm{BZ}} \Omega(\mathbf{k})d^2k$ and $\Omega(\mathbf{k})$ is the Berry curvature over all the occupied states [53,54],

$$\Omega(\mathbf{k}) = \sum_{n<E_F}\sum_{m\neq n} 2\mathrm{Im}\frac{\langle\psi_{n\mathbf{k}}|\upsilon_x|\psi_{m\mathbf{k}}\rangle\langle\psi_{m\mathbf{k}}|\upsilon_y|\psi_{n\mathbf{k}}\rangle}{(\varepsilon_{m\mathbf{k}}-\varepsilon_{n\mathbf{k}})^2}, \quad (1)$$

where m, n are band indices, $\psi_{m/n\mathbf{k}}$ and $\varepsilon_{m/n\mathbf{k}}$ are the Bloch wave functions and corresponding eigenenergies of band m/n, respectively, and $\upsilon_{x/y}$ are the velocity operators. The left panel of Fig. 2(d) shows the σ_{xy}^{A} relative to the Fermi level and the reciprocal-space distribution of Berry curvature for whole valence bands. The calculated Berry curvature is almost zero except around the Γ point. Integrating the Berry curvatures, as expected, σ_{xy}^{A} shows a quantized value with $\mathcal{C} = 1$ when Fermi level is inside the energy window of SOC gap, confirming the QAH state. For further experimental investigations and device applications, we then focus on the substrate effect due to the fact that a free-standing film is usually hard to grow. Remarkably, both the insulating and topological properties are preserved on a lattice matching substrate [52].

The existence of an intrinsic QAH phase in FM $EuCd_2As_2$ QLs offers an intriguing platform to scrutinize the possibility of realizing the topological phase transition as well as magnetic topological states, and their external control, which is critical for both fundamental investigations and practical applications. The electric-field-induced topological phase transition between topological and conventional insulator has been theoretically predicted and experimentally verified and been proposed as the basis of a topological field effect transistor [33–36]. Here, we show that a perpendicular electric field can even be used to control the topological characters between two topological states in $EuCd_2As_2$ QLs, and a $\mathcal{T}$-broken QSH insulator with gapless edge states can indeed be generated. To get preliminary insight into the electric-field-induced topological phase transition, Fig. 3(a) presents the variation in global energy gaps (marked by the squares) with SOC as the electric field is varied. There is a crossover from a direct to an indirect gap and the global energy gaps decrease when an electric field is introduced, illustrated also in Fig. 3(c). A further increase of the electric field leads to negative values when $E > E_a$, i.e., a nontrivial insulator-to-metal transition, and a closure of the gap occurs at the peak position ($E = E_b$) of the negative values. Remarkably, an energy gap reopens across the peak position and an insulator is reproduced with $E > E_c$. Generally, the process of energy gap closing and reopening reveals a topological phase transition.

To determine the band topology of these electric-field-induced magnetic insulators, we use $E = 0.2$ V/Å as an example, for which the out-of plane ferromagnetism survives to be energetically favorable and therefore the spin polarization remains in the absence of SOC as presented in Figs. 4(a) and 4(b). However, different from the configuration without an electric field, here both of the spin-up and spin-down bands are gapless. After including SOC, shown in Fig. 4(c), a global energy gap with a positive value of 35 meV opens. We then check the anomalous Hall conductivity σ_{xy}^{A}. Figure 4(d) shows $\sigma_{xy}^{A} = 0$, i.e., $\mathcal{C} = 0$, for bands below the SOC-induced gap; hence the QAHE cannot be realized. Interestingly, similar

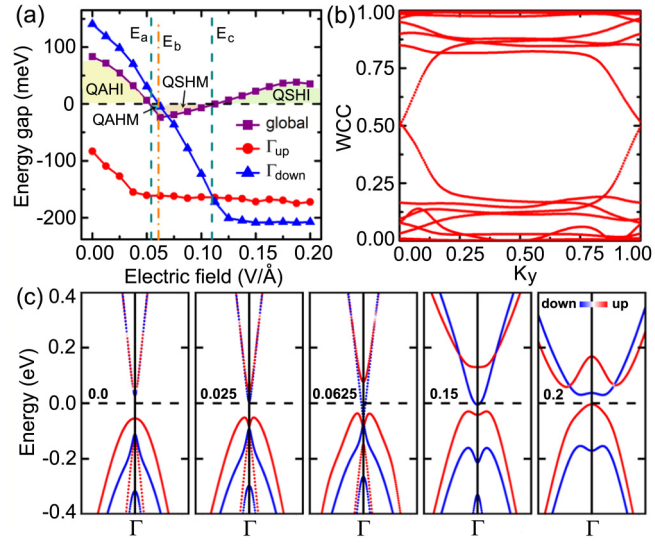

FIG. 3. (a) Variation of global energy gaps and energy gaps at Γ for spin-up and spin-down subbands in FM $EuCd_2As_2$ QLs versus the perpendicular electric field E. A topological phase transition occurs accompanied by a gap closing-reopening process for spin-down subbands while the topology remains because the gap survives for spin-up subbands. (b) Evolution of Wannier charge centers (WCC) along k_y with $E = 0.2$ V/Å. (c) Band structure evolution of FM $EuCd_2As_2$ QLs with SOC as a function of E. Spin-up and spin-down subbands are denoted by colors from red to blue with the expectation value of the σ_z in the basis of MLWFs.

to graphene [12], SOC opens a gap for both spin-up and spin-down subbands (that are degenerate in graphene), in $EuCd_2As_2$ QLs under $E = 0.2$ V/Å, inspiring us to check the spin Hall conductivity $\sigma_{xy}^{S} = \frac{e\hbar}{(2\pi)^2}\int_{\mathrm{BZ}} \Omega^{S}(\mathbf{k})d^2k$ with $\Omega^{S}(\mathbf{k})$ is the spin Berry curvature of all occupied states, as well as the spin Chern number $\mathcal{C}_S$, defined as $\mathcal{C}_S = (\mathcal{C}_+ - \mathcal{C}_-)/2$, where $\mathcal{C}_+$ and $\mathcal{C}_-$ are Chern numbers of spin-up and spin-down manifolds, which characterize the QSH insulator even without $\mathcal{T}$ [39]. When the Fermi level is located within the SOC-induced energy gap, as shown in Fig. 4(d), the σ_{xy}^{S} of all occupied states indeed acquires a quantized value of 2, in excellent agreement with the calculated integer value $\mathcal{C}_S = 1$ with the alternative representation $\sigma_{xy}^{S} = 2\mathcal{C}_S\frac{e}{4\pi}$ [39], indicating the $\mathcal{T}$-broken QSH effect in $EuCd_2As_2$ QLs. The $\mathcal{T}$-broken QSH state is further explicitly confirmed by the Wannier charge centers as presented in Fig. 3(b) [55]. Thus, a topological phase transition from QAH effect to $\mathcal{T}$-broken QSH effect can be effectively tuned by electric field.

To better understand this intriguing topological phase transition, we distinguish the spin-up and spin-down bands with SOC by matrix elements of the Pauli matrices σ_z, $\langle\psi_{m\mathbf{k}}|\sigma_z|\psi_{n\mathbf{k}}\rangle$, on the basis of MLWFs with the first-principles bands were accurately reproduced. Their energy gaps at the Γ point and band structure evolution are illustrated in Figs. 3(a) and 3(c), respectively, as the electric field is varied. The negative values indicate the inverted energy gaps. The energy gaps of spin-up and spin-down subbands respond differently to electric field. The conduction and valance bands approach each other and the energy gaps decrease for the spin-down subbands when an electric field is introduced. A further

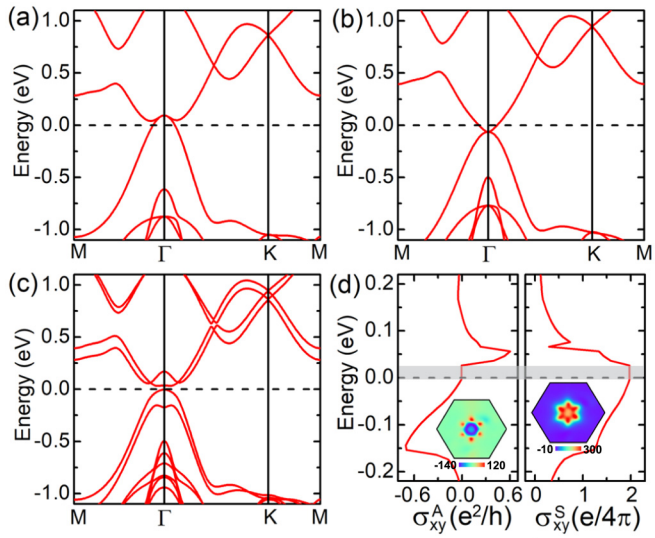

FIG. 4. Band structures of $EuCd_2As_2$ QLs under an electric field of 0.2 V/Å (a), (b) without SOC and (c) with SOC. Both the (a) spin-up and (b) spin-down bands are gapless. (d) Anomalous Hall conductivity σ^A_{xy} and spin Hall conductivity σ^S_{xy} with respect to the position of the Fermi energy E_F. Insets are Berry curvature and spin Berry curvature in the Brillouin zone. σ^A_{xy} goes to zero while a quantized value in the SOC gap is obtained for σ^S_{xy}.

increase of the electric field leads to an energy gap closing and reopening, indicating that a topological phase transition occurs for spin-down subbands around $E_b = 0.06\ V/Å$. The energy gaps of spin-up subbands always open, implying that the phase is not changed. To identify the topological natures, $E = 0.0\ V/Å$ and $E = 0.2\ V/Å$ are chosen as examples and the corresponding Chern numbers of spin-up and spin-down subbands, $\mathcal{C}_\pm$, are calculated. For $E = 0.0\ V/Å$, the Chern numbers are, respectively, $\mathcal{C}_+ = 1$ and $\mathcal{C}_- = 0$, yielding the total Chern number $\mathcal{C} = 1$ and the spin Chern number $\mathcal{C}_\mathcal{S} = 1/2$, in agreement with the results of σ^A_{xy} and σ^S_{xy} as shown in Fig. 2(d). Thus, we may refer the $EuCd_2As_2$ QLs as quantum spin Chern insulator due to the coexistence of nonzero $\mathcal{C}$ and $\mathcal{C}_\mathcal{S}$ [56]. The $\mathcal{C}_+$ remains unchanged with $\mathcal{C}_+ = 1$ while $\mathcal{C}_-$ changes from $\mathcal{C}_- = 0$ to $\mathcal{C}_- = -1$ when E changes to $E = 0.2\ V/Å$, meaning that the band topology appears in the spin-down subband and leading to $\mathcal{C} = 0$ and $\mathcal{C}_\mathcal{S} = 1$. Therefore, a topological phase transition occurs in spin-down subbands but not in spin-up subbands, resulting in the $\mathcal{T}$-broken QSH effect from the QAH effect in $EuCd_2As_2$ QLs.

Another prominent feature of QAH and QSH insulators is the existence of metallic edge states that are of chiral and helical nature, respectively. Eventually, to complement and

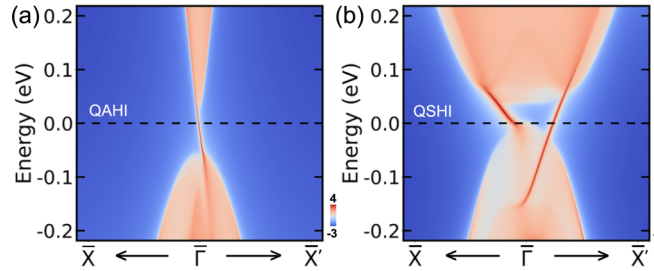

FIG. 5. Band structures of a $EuCd_2As_2$ nanoribbon terminated by zigzag chains of Cd and As atoms in (a) the QAH phase and (b) the $\mathcal{T}$-broken QSH phase. Unlike the conventional QSH effect, breaking $\mathcal{T}$ causes only the edge states to shift in momentum space but not open a gap.

further check the topological phase transition, we performed calculations of the edge state of a semi-infinite nanoribbon using MLWFs [55]. Figure 5 displays the edge states of a $EuCd_2As_2$ nanoribbon terminated by zigzag chains of Cd and As atoms. Within the gap, one can clearly see that one chiral edge state connects the conduction and valence bands, that is consistent with the calculated Chern number $\mathcal{C} = 1$ for $EuCd_2As_2$ QLs without electric field, Fig. 5(a). In contrast, for $EuCd_2As_2$ QLs under $E = 0.2\ V/Å$, each subband exhibits an independent QAH effect with a nonzero Chern number $\mathcal{C}_\pm = \pm 1$, but the spin-up and spin-down edge states are decoupled with opposite chirality due to the breaking of $\mathcal{T}$. Therefore, a single pair of anisotropic helical edge states is obtained as shown in Fig. 5(b), and remarkably, different from the conventional QSH effect, breaking $\mathcal{T}$ causes only the edge states to shift in momentum space but not opens a gap.

In summary, we demonstrated the emergence of QAH effect in a stable 2D FM insulator, $EuCd_2As_2$ QLs, which presents a sizable nontrivial gap of 72 meV and $\mathcal{C}$ number of chiral edge states. Under electric field, the spin-up and spin-down subbands are tunable oppositely, and an exotic topological state, $\mathcal{T}$-broken QSH insulator, that is different from the conventional one, can be obtained. Ultimately, the presented results greatly advance our general understanding of the topological effects and phase transitions in 2D magnetic materials and hence intrigue forward experimental interest and potential applications in spintronics.

This work is supported by the Natural Science Foundation of Shandong Province (Grants No. ZR2019QA019 and No. ZR2019MEM013), Taishan Scholar Program of Shandong Province. We also thank the Qilu Young Scholar Program of Shandong University.

[1] L. Šmejkal, Y. Mokrousov, B. Yan, and A. H. MacDonald, Nat. Phys. **14**, 242 (2017).
[2] Y. Tokura, K. Yasuda, and A. Tsukazaki, Nat. Rev. Phys. **1**, 126 (2019).
[3] M. Z. Hasan and C. L. Kane, Rev. Mod. Phys. **82**, 3045 (2010).
[4] X.-L. Qi and S.-C. Zhang, Rev. Mod. Phys. **83**, 1057 (2011).
[5] A. Bansil, H. Lin, and T. Das, Rev. Mod. Phys. **88**, 021004 (2016).
[6] K. v. Klitzing, G. Dorda, and M. Pepper, Phys. Rev. Lett. **45**, 494 (1980).
[7] F. D. M. Haldane, Phys. Rev. Lett. **61**, 2015 (1988).

[8] H. Weng, R. Yu, X. Hu, X. Dai, and Z. Fang, Adv. Phys. **64**, 227 (2015).

[9] Y. Ren, Z. Qiao, and Q. Niu, Rep. Prog. Phys. **79**, 066501 (2016).

[10] C.-X. Liu, S.-C. Zhang, and X.-L. Qi, Annu. Rev. Condens. Matter Phys. **7**, 301 (2016).

[11] B. A. Bernevig, T. L. Hughes, and S.-C. Zhang, Science **314**, 1757 (2006).

[12] C. L. Kane and E. J. Mele, Phys. Rev. Lett. **95**, 226801 (2005).

[13] X.-L. Qi, Y.-S. Wu, and S.-C. Zhang, Phys. Rev. B **74**, 085308 (2006).

[14] C.-X. Liu, X.-L. Qi, X. Dai, Z. Fang, and S.-C. Zhang, Phys. Rev. Lett. **101**, 146802 (2008).

[15] R. Yu, W. Zhang, H.-J. Zhang, S.-C. Zhang, X. Dai, and Z. Fang, Science **329**, 61 (2010).

[16] Z. Qiao, S. A. Yang, W. Feng, W.-K. Tse, J. Ding, Y. Yao, J. Wang, and Q. Niu, Phys. Rev. B **82**, 161414(R) (2010).

[17] H. Zhang, C. Lazo, S. Blügel, S. Heinze, and Y. Mokrousov, Phys. Rev. Lett. **108**, 056802 (2012).

[18] J. Wang, B. Lian, H. Zhang, Y. Xu, and S.-C. Zhang, Phys. Rev. Lett. **111**, 136801 (2013).

[19] X. Liu, H.-C. Hsu, and C.-X. Liu, Phys. Rev. Lett. **111**, 086802 (2013).

[20] H. Zhang, Y. Xu, J. Wang, K. Chang, and S.-C. Zhang, Phys. Rev. Lett. **112**, 216803 (2014).

[21] S.-C. Wu, G. Shan, and B. Yan, Phys. Rev. Lett. **113**, 256401 (2014).

[22] Z. Qiao, W. Ren, H. Chen, L. Bellaiche, Z. Zhang, A. H. MacDonald, and Q. Niu, Phys. Rev. Lett. **112**, 116404 (2014).

[23] G. Xu, J. Wang, C. Felser, X. L. Qi, and S. C. Zhang, Nano Lett. **15**, 2019 (2015).

[24] C. Niu, G. Bihlmayer, H. Zhang, D. Wortmann, S. Blügel, and Y. Mokrousov, Phys. Rev. B **91**, 041303(R) (2015).

[25] Z. F. Wang, Z. Liu, J. Yang, and F. Liu, Phys. Rev. Lett. **120**, 156406 (2018).

[26] C.-Z. Chang, J. Zhang, X. Feng, J. Shen, Z. Zhang, M. Guo, K. Li, Y. Ou, P. Wei, L.-L. Wang, Z.-Q. Ji, Y. Feng, S. Ji, X. Chen, J. Jia, X. Dai, Z. Fang, S.-C. Zhang, K. He, Y. Wang, L. Lu, X.-C. Ma, and Q.-K. Xue, Science **340**, 167 (2013).

[27] J. G. Checkelsky, R. Yoshimi, A. Tsukazaki, K. S. Takahashi, Y. Kozuka, J. Falson, M. Kawasaki, and Y. Tokura, Nat. Phys. **10**, 731 (2014).

[28] S.-Y. Xu, Y. Xia, L. A. Wray, S. Jia, F. Meier, J. H. Dil, J. Osterwalder, B. Slomski, A. Bansil, H. Lin, R. J. Cava, and M. Z. Hasan, Science **332**, 560 (2011).

[29] T. Sato, K. Segawa, K. Kosaka, S. Souma, K. Nakayama, K. Eto, T. Minami, Y. Ando, and T. Takahashi, Nat. Phys. **7**, 840 (2011).

[30] C. Niu, P. M. Buhl, G. Bihlmayer, D. Wortmann, S. Blügel, and Y. Mokrousov, Nano Lett. **15**, 6071 (2015).

[31] C. Liu, W. Gao, B. Yang, and S. Zhang, Phys. Rev. Lett. **119**, 183901 (2017).

[32] S. Murakami, M. Hirayama, R. Okugawa, and T. Miyake, Sci. Adv. **3**, e1602680 (2017).

[33] X. Qian, J. Liu, L. Fu, and J. Li, Science **346**, 1344 (2014).

[34] Q. Liu, X. Zhang, L. B. Abdalla, A. Fazzio, and A. Zunger, Nano Lett. **15**, 1222 (2015).

[35] W. G. Vandenberghe and M. V. Fischetti, Nat. Commun. **8**, 14184 (2017).

[36] J. L. Collins, A. Tadich, W. Wu, L. C. Gomes, J. N. B. Rodrigues, C. Liu, J. Hellerstedt, H. Ryu, S. Tang, S.-K. Mo, S. Adam, S. A. Yang, M. S. Fuhrer, and M. T. Edmonds, Nature (London) **564**, 390 (2018).

[37] T. Zhou, J. Zhang, B. Zhao, H. Zhang, and Z. Yang, Nano. Lett. **15**, 5149 (2015).

[38] M. Ezawa, Phys. Rev. Lett. **109**, 055502 (2012).

[39] Y. Yang, Z. Xu, L. Sheng, B. Wang, D. Y. Xing, and D. N. Sheng, Phys. Rev. Lett. **107**, 066602 (2011).

[40] G. Kresse and J. Hafner, Phys. Rev. B **47**, 558 (1993).

[41] G. Kresse and J. Furthmüller, Phys. Rev. B **54**, 11169 (1996).

[42] See http://www.flapw.de.

[43] J. P. Perdew, K. Burke, and M. Ernzerhof, Phys. Rev. Lett. **77**, 3865 (1996).

[44] A. Togo and I. Tanaka, Scr. Mater. **108**, 1 (2015).

[45] A. A. Mostofi, J. R. Yates, Y.-S. Lee, I. Souza, D. Vanderbilt, and N. Marzari, Comput. Phys. Commun. **178**, 685 (2008).

[46] F. Freimuth, Y. Mokrousov, D. Wortmann, S. Heinze, and S. Blügel, Phys. Rev. B **78**, 035120 (2008).

[47] M. C. Rahn, J.-R. Soh, S. Francoual, L. S. I. Veiga, J. Strempfer, J. Mardegan, D. Y. Yan, Y. F. Guo, Y. G. Shi, and A. T. Boothroyd, Phys. Rev. B **97**, 214422 (2018).

[48] G. Hua, S. Nie, Z. Song, R. Yu, G. Xu, and K. Yao, Phys. Rev. B **98**, 201116(R) (2018).

[49] A. Artmann, A. Mewis, M. Roepke, and G. Michels, Z. Anorg. Allg. Chem. **622**, 679 (1996).

[50] I. Schellenberg, U. Pfannenschmidt, M. Eul, C. Schwickert, and R. Pöttgen, Z. Anorg. Allg. Chem. **637**, 1863 (2011).

[51] T. Björkman, A. Gulans, A. V. Krasheninnikov, and R. M. Nieminen, Phys. Rev. Lett. **108**, 235502 (2012).

[52] See Supplemental Material at http://link.aps.org/supplemental/10.1103/PhysRevB.99.235119 for molecular dynamics calculations, crystal and electronic structures.

[53] D. J. Thouless, M. Kohmoto, M. P. Nightingale, and M. den Nijs, Phys. Rev. Lett. **49**, 405 (1982).

[54] Y. Yao, L. Kleinman, A. H. MacDonald, J. Sinova, T. Jungwirth, D. S. Wang, E. Wang, and Q. Niu, Phys. Rev. Lett. **92**, 037204 (2004).

[55] Q. Wu, S. Zhang, H.-F. Song, M. Troyer, and A. A. Soluyanov, Comput. Phys. Commun. **224**, 405 (2018).

[56] H. Zhang, F. Freimuth, G. Bihlmayer, M. Ležaić, S. Blügel, and Y. Mokrousov, Phys. Rev. B **87**, 205132 (2013).